

Potential for > 1 THz observing with ALMA

Sarah Graves & John Richer
Cavendish Laboratory, Cambridge

August 15, 2014

Abstract

As part of the ESO-funded Band 11 study, this report examines the site conditions and expected sensitivities of ALMA for frequencies in the THz range of 1000-1600 GHz.

The distribution of extremely dry weather (as measured by the precipitable water vapour) on the ALMA site is measured through site testing data (1995-2004) and the observations of APEX (2006 to current day).

The expected atmospheric transmission and sky brightness at these wavelengths has been modelled using the AM code. Using these data, as well as estimates of the telescope performance, the sensitivity of ALMA has been calculated for a range of possible receiver temperatures, configurations and weather conditions.

Finally, some simple imaging simulations have been created using the CASA `sim` toolkit, by extending the `simobs` and `simanalyze` tasks within CASA to work at THz frequencies.

1. Site conditions

1.1. PWV

The primary way to characterise the atmospheric transparency above the ALMA site is through measurements of the Precipitable Water Vapour, which we will refer to as PWV. This has been calculated indirectly through historic 225 GHz opacity measurements taken with a tipping radiometer between 1996 and 2004¹, and more recently (and more directly) through radiometer measurements of the 183 GHz water line taken by APEX.

1.2. Tipping Radiometer

Measurements of the 225 GHz opacity τ_{225} were taken as part of the site testing. These data were taken approximately every ten minutes between 1996 and 2004, but there are extended periods during this time when the equipment was not functioning.

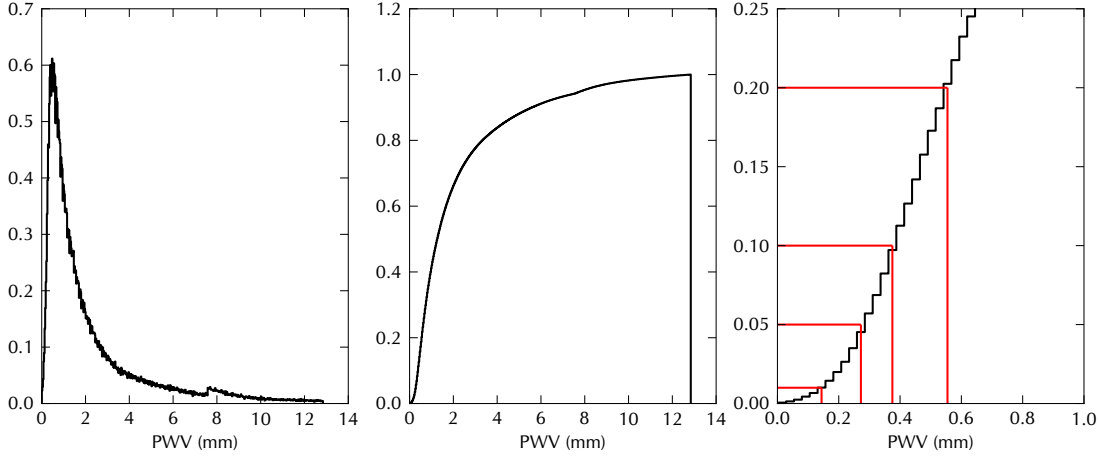
To analyse this data, the times when the measurements report `-999` were removed, and all values of $\tau_{225} > 1e8$ were also removed, as were values measured with erroneous dates (i.e. times greater than 24 hours). Additionally, based on the analysis of the data in ALMA Memo 333, the data with values of τ_{225} greater than 0.5 are not included – these data may be taken when the telescope is moving, or similar other erroneous situation.

We have used the AM software package written by Scott Paine (SMA Memo 152, retrieved from <http://www.cfa.harvard.edu/sma/memos/152.pdf>) to carry out radiative transfer calculations through the atmosphere. In particular, we used AM to

¹<http://www.submm.caltech.edu/~sradford/site-eval/225trans.html>

Table 1: PWV percentiles for the ALMA site, based on site testing data from 1996-2004.

Percentile	PWV (mm)
20%	0.55
10%	0.37
5%	0.27
1%	0.14


Figure 1: Histograms of the PWV-derived τ_{225} between 1995 and 2004. Left: Normalised histogram, Center: Cumulative histogram, Right: zoom in on good weather end of cumulative histogram, with 10%, 5%, 1% and 0.5% percentiles indicated.

establish the conversion of τ_{225} to PWV values, for an atmosphere appropriate to Chajnantor, finding:

$$PWV = \frac{\tau_{225} - 0.012}{0.038} \quad (1)$$

A histogram of the PWV values is shown in Fig. 1. The 20% level is at PWV=0.55 mm, 10% at PWV=0.37, 5% at 0.27 and 1% at 0.14 mm.

The variation in PWV over the years studied is shown in Fig. 2 (using the median value for each month), and the fraction of samples in each month taken with PWV < 0.5 mm is also shown in. Its important to note that as well as the expected seasonal variation with better weather in the winter, and very poor weather during the ‘Bolivian winter’ early on in the year, there will be significant variation in the quantity of good weather found in different years.

1.3. APEX 183 GHz radiometer

Additionally, APEX (on the same site) has a 183 GHz radiometer and they have kindly sent their 1 minute sampled values for the PWV, taken at the times the telescope is observing, from 2006 up until December 2012. These values should be more accurate, but are less complete. However, assuming APEX is more likely to be observing during the best weather, we can assume that this will be a reasonably complete sampling of the driest weather which we are interested in for THz observing.

Table 2 shows the hours per year that the APEX radiometer observed weather with a PWV < 0.5, 0.3, and 0.2 mm. (Note that the 0.5 mm count includes all the hours with weather better than 0.3 and 0.2 mm). These were calculated after median smoothing the 1-minute sampled data points within a 20 minute window.

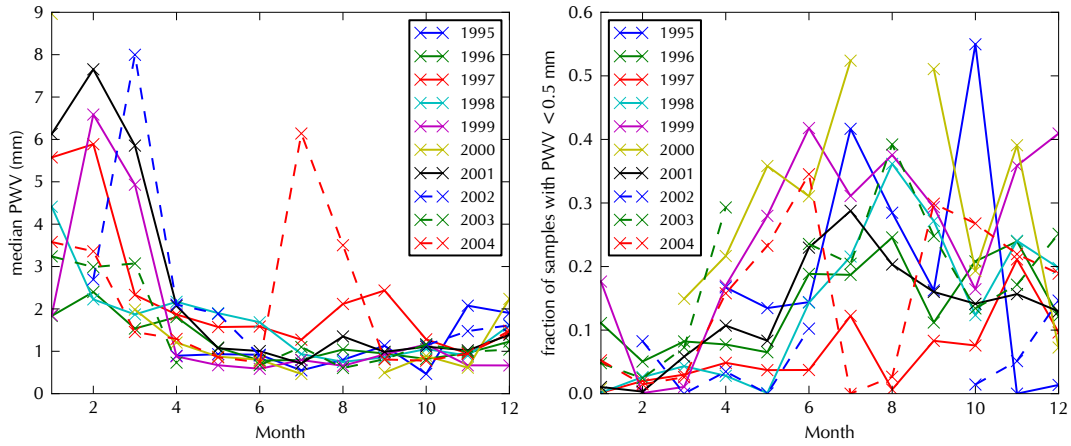


Figure 2: PWV variation over the years studied. Left: the pwv shown is the median value for each month (anomalous high values from 2004 may be due to very little data being taken then). Right: The values plotted is the fraction of samples taken with PWV < 0.5 mm.)

Table 2: The number of hours APEX observed with a PWV of less then 0.5,0.3, 0.2 and 0.1 mm, per year. Also shown for comparison is the total number of hours for which PWV data are available for each year.

Year	Total hrs	PWV (mm)			
		<0.5	<0.3	<0.2	<0.1
2006	3731	787	214	64	29
2007	5675	1043	301	84	36
2008	6575	2027	826	393	184
2009	6753	1169	273	73	9
2010	7514	1938	661	178	35
2011	6084	1356	497	228	48
2012	6621	1331	421	123	21

One potential issue for observing at these wavelengths is determining if the extremely dry weather required for these observations is found in long enough continuous periods to permit reasonably long observations. Fig. 3 shows the PWV variation with time, median smoothed over a 20 minute window to remove individual spikes. (Note that 2008 appears to have had exceptionally dry weather in the middle of the year.)

Fig. 4 shows as an example a good weather month featuring a large amount of dry nights of observing (October 2010). Based on these plots, it does seem that we will be able to expect a reasonable number of nights with long (multi-hour) stretches of weather with $PWV < 0.3$ mm, within the driest observing months. As seen from the historical data, there will be considerable variation from year to year in the number of hours of potential observing for these weather conditions.

2. Atmospheric modelling at THz frequencies

The atmospheric transmission and transparency at THz wavelengths has been modelled using the code `am` written by Scott Paine of CfA. The default `am` setup for Chajnantor is used. This model defines layers within a given pressure range, and gives the temperature, water, dry air and ozone values for each layer (note that a water value is only provided for the bottom 5 layers, up to 280 mbar of pressure – the model ignores the small amount of water in the stratosphere).

The user supplies the temperature of the base layer (this will not affect higher layers). The user also provides a total PWV value, this is used to scale the water values provided for the layers.

This uses H_2O , dry air and O_3 profiles. Each layer has the pressure at the base of layer, the temperature at base of layer (scaled by ground temperature), a hydrostatic dry air column and an O_3 hydrostatic profile. In addition, the bottom 5 layers have an H_2O profile (scaled by the given PWV value).

The following sky brightness and atmospheric transmission graphs have been produced from these simulations, assuming a ground temperature of 270 K (the mean at the ALMA site). The effect of the zenith angle on the atmospheric transmission has also been included: Fig. 5 shows the variation in the atmospheric transmission for angles of between 0 and 30 degrees at 270 K ground temperature. Fig. 6 shows close ups on the three THz windows in the 1-1.6 THz range. There are large number of absorption features visible throughout these bands.

The sky brightness throughout these bands is also produced by these models. Fig. 7 shows the Rayleigh-Jeans brightness temperature of the sky at these frequencies.

3. System Temperatures

The system temperature for a telescope can be expressed as:

$$T_{\text{sys}} = T_{\text{rx}} + \eta_{\text{ff}} T_{\text{b,sky}} + (1 - \eta_{\text{ff}}) T_{\text{amb}} \quad (2)$$

where all the temperatures are Rayleigh-Jeans brightness temperatures, T_{sys} is the system temperature, T_{rx} is the receiver temperature, η_{ff} is the forward efficiency (fraction of antenna power pattern in main beam), $T_{\text{b,sky}}$ is the Rayleigh-Jeans brightness temperature of the sky (including CMB, at a specific frequency and zenith), and T_{amb} is the ambient temperature seen by the spillover fraction of the antenna power pattern.

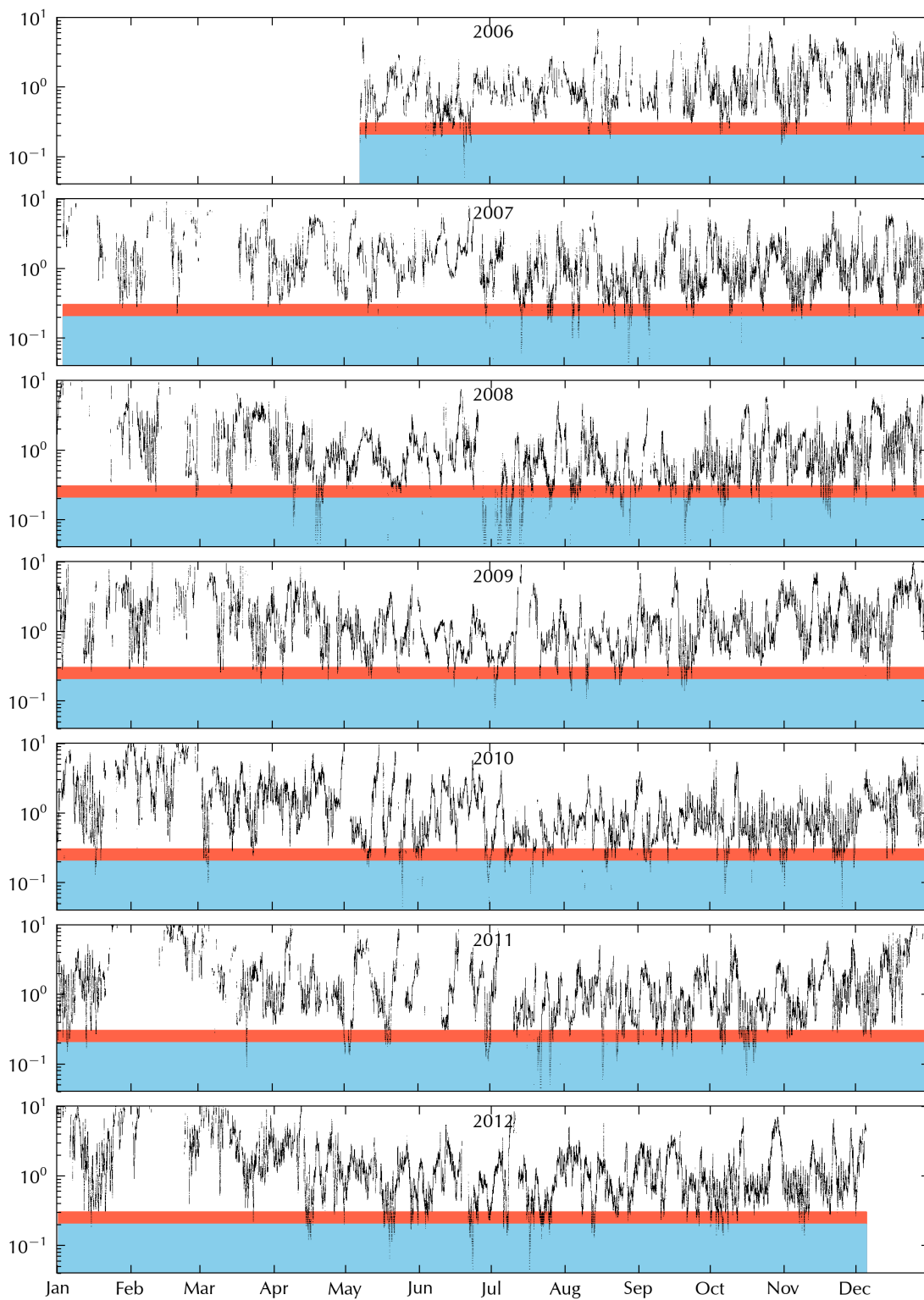


Figure 3: PWV measurements from APEX for 2006-2012, median smoothed within a 20 minute window. The red region shaded region indicates PWVs of less than 0.3mm water, and the blue region indicates PWVs of less than 0.2 mm.

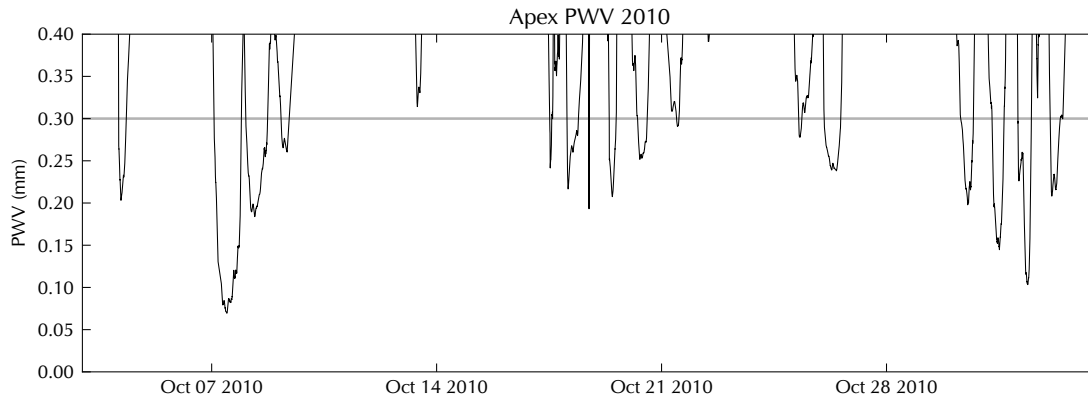


Figure 4: A zoom in on the best weather conditions found within October 2010. Note that there appears to be several nights of potential THz observing during this time period.

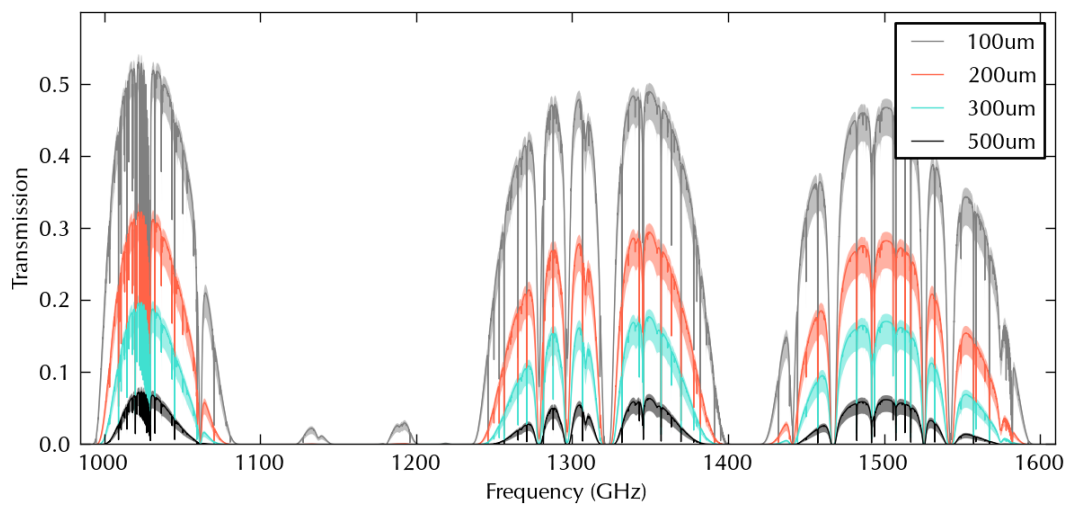


Figure 5: AM modelled transmittance at ALMA site through 1-1.6 THz, for varying PWV values. The shaded regions indicate the variation for zenith angles of 0-30 degrees; the line indicates transmittance at 15 degrees zenith.

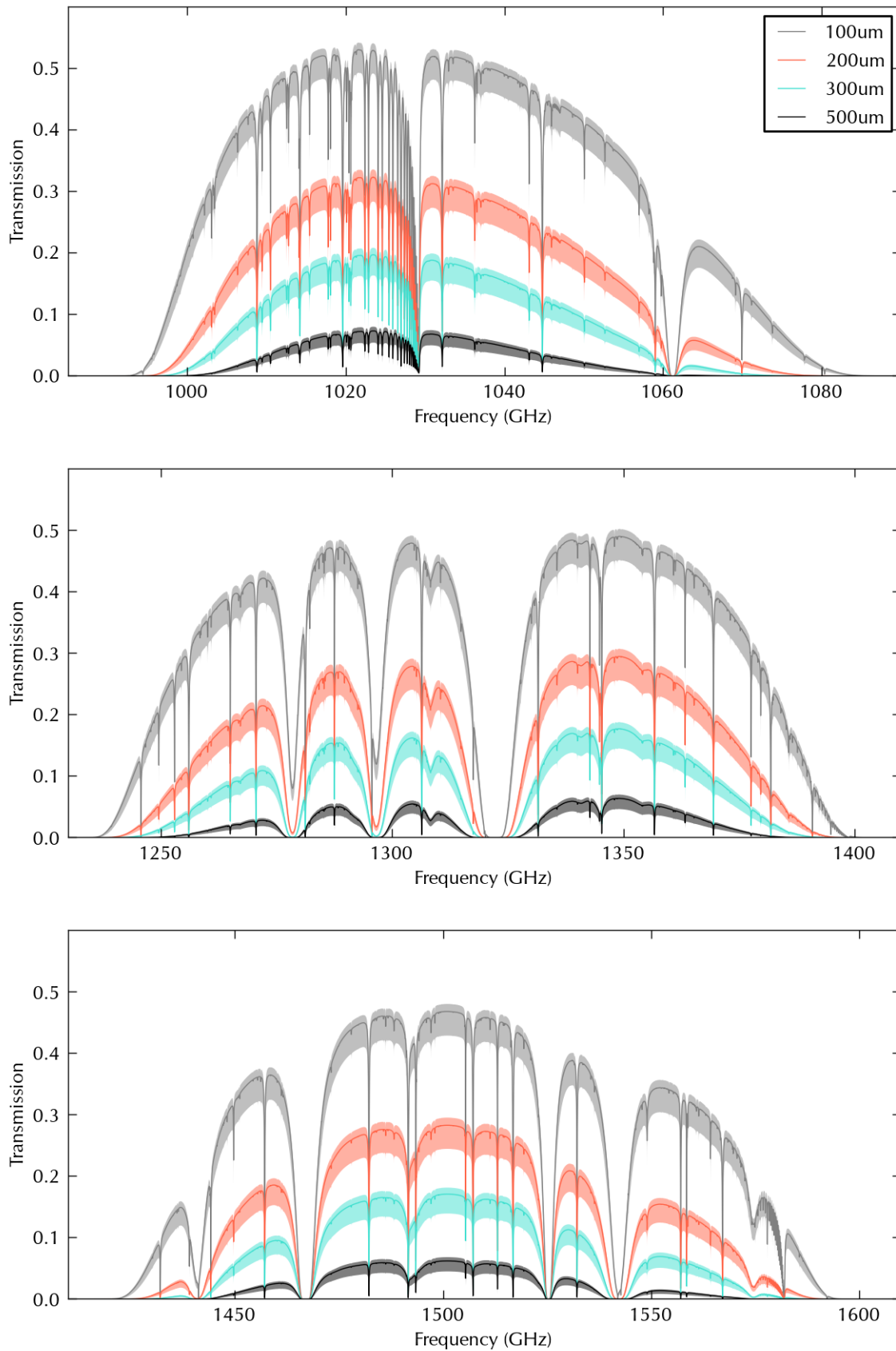


Figure 6: AM modelled transmittance in the three THz windows under consideration here. The shaded regions indicate the transmittance between 0 and 30 degrees zenith angle for each specific PWV value; the solid lines indicate the transmission for a 15 degrees zenith for each PWV value.

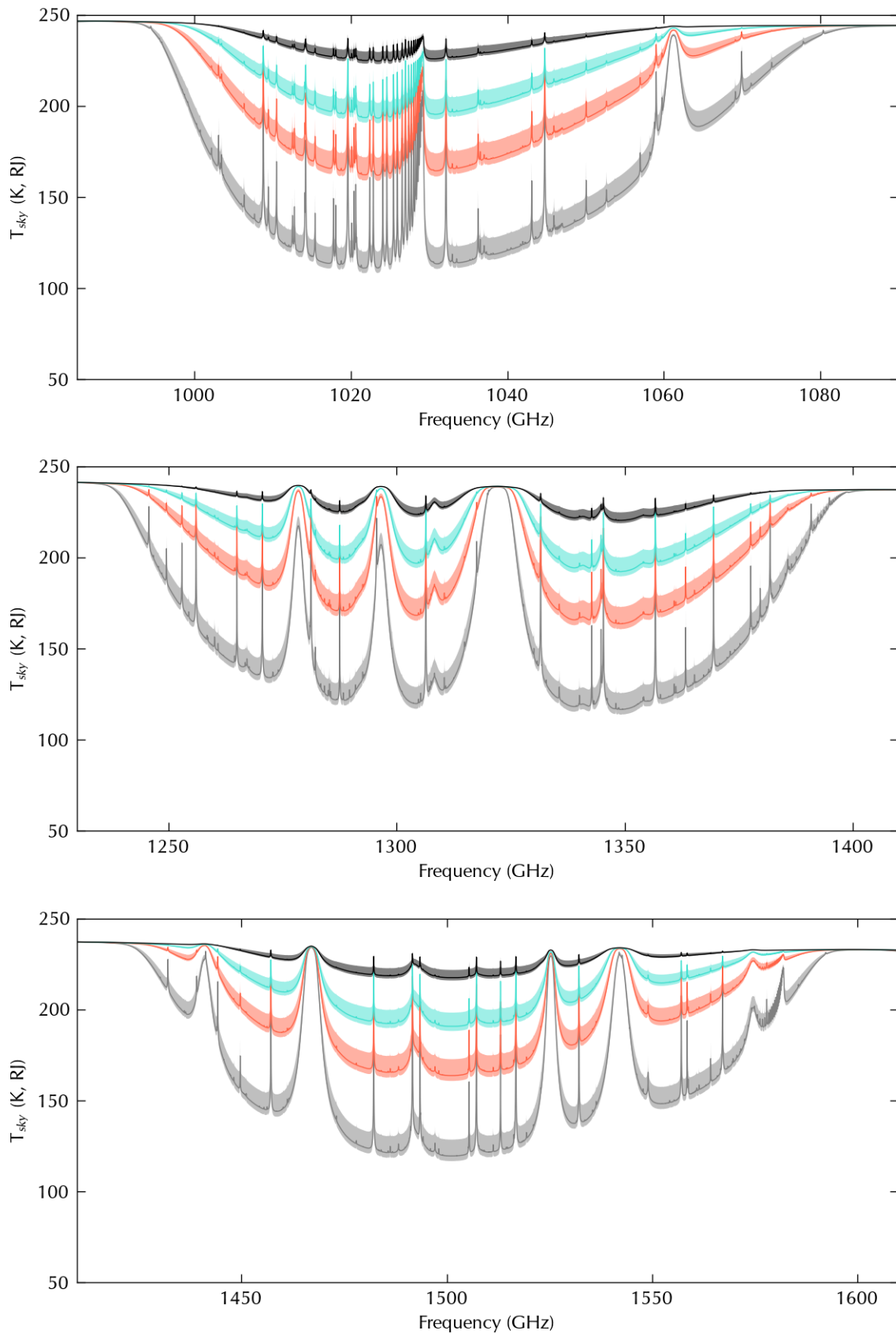


Figure 7: AM modelled sky brightness temperature for Chajnantor, converted to Rayleigh-Jeans brightness temperatures, for the three THz windows in the 1-1.6 THz frequency range. The shaded regions indicate the 0-30 degree zenith variation, and the solid lines indicate the 15 degree zenith angle values for each different PWV value that has been modelled. The PWV values are indicated by the same colours as in Fig.6.

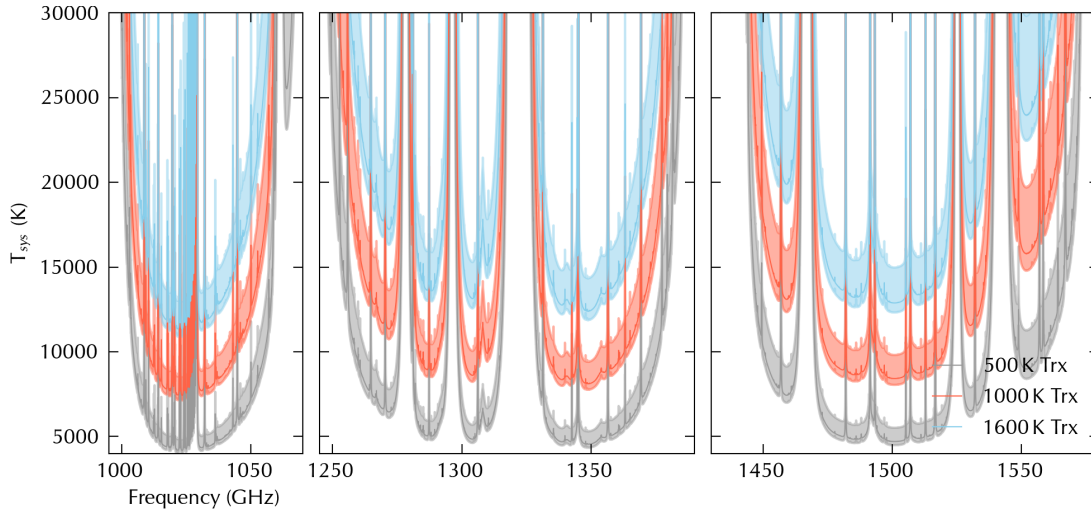


Figure 8: Estimated system temperatures for weather of 200 μm PWV, for a source at 15 degrees zenith angle, for 500, 1000 and 1600 K receiver temperatures.

If we wish to reference this temperature scale to a point outside the atmosphere, then the effective system temperature is $T_{\text{sys}}/\eta_{\text{ff}}t_x$ where $t_x = e^{-\tau_v}$ is the transmittance.

The transmittance and the sky brightness temperature for a given PWV, ground temperature and zenith angle have been calculated by AM. The median ambient temperature at ALMA has been measured as 270 K.

The equation used for ALMA by the ALMA sensitivity Calculator² is

$$T_{\text{sys}} = (1 + g) \frac{(T_{\text{rxrj}} + \eta_{\text{eff}}T_{\text{skyrj}} + (1 - \eta_{\text{eff}})T_{\text{ambrrj}})}{\eta_{\text{eff}}t_x} \quad (3)$$

This is the same as Eqn. 2 above, except it includes an additional factor of $(1 + g)$ to distinguish between single and double sideband receiver systems. For single sideband, $g = 0$, and for double sideband $g = 1$. This report assumes that any THz receiver system would be double sideband.

3.1. Receiver Temperature

Estimates of what receiver temperatures will be possible at these band widths in the future are difficult to predict. The current THz receiver temperatures found within the literature are as low as 1600 K for current, functioning instrumentation. GREAT on *SOFIA* has achieved receiver noise temperatures of ~ 1600 K for the 1.25-1.5 THz receivers, and 2100 K for 1.82-1.92 THz.³ APEX has achieved temperatures of ~ 1600 K DSB receiver temperatures across the band 1.25-1.53 THz (Wiedner 2006: A&A 454 L33). The initial proposal for funding for this THz ALMA study suggested DSB noise temperatures of 1000 K could be expected in the 1.3THz and 1.5THz regions. The tables of calculated system sensitivities given in this work use values of 1000 K and 800 K.

²See: <http://almascience.eso.org/documents-and-tools/alma-technical-handbook>, A. Lundgren, 2012, ALMA Cycle 1 Technical Handbook, Version 1.01, ALMA; Chapter 8 sensitivity calculator

³http://www.sofia.usra.edu/Science/instruments/instruments_great.html

3.2. Additional Factors

There are numerous additional factors that can reduce the sensitivity of the system. Decorrelation of the signal is caused by residual phase errors from atmospheric phase. Errors in the antenna surfaces and phase noise from the local oscillator are also potential sources of difficulty.

Flux calibration of the observations may also be an issue at these frequencies, particularly for high resolution observations. Discussions with those who have operated THz instruments from Mauna Kea, Chajnantor and Sairecabur suggest flux uncertainties of tens of per cent are often present depending on the stability of the weather, and on the observing airmass. Accurate and rapid WVR systems on ALMA antennas should help improve this as long as the atmospheric models can be well enough understood, and experience with Band 10 will be important in quantifying how hard this will be.

3.2.1. Ruze efficiency

The smoothness of the antenna surface affects the point source sensitivity of the antennas by effectively decorrelating some of the signal from the errors in the surface. The Ruze efficiency can be used to calculate the equivalent effective antenna area for a given surface error:

$$A_{\text{eff}} = AR_0 e^{-(4\pi\sigma\nu/c)^2} \quad (4)$$

where A is the geometrical area (113.1 for the 12-m, 38.5 m² for the 7 m), $R_0=0.72$ (from ALMA technical handbook for cycle 1, chapter 8), σ is the surface error of the antenna, ν is the frequency of the observation, c is the speed of light and A_{eff} is the effective area of the antenna to be used in the sensitivity calculation.

The specification for ALMA requires a smoothness of 25 μm for 12 m antennas and 20 μm for the 7 m antennas. In practice, some of the antennas have been found to exceed this specification – potentially as good as 13 μm for the 7 m antennas and better than 18 μm for some of the 12 m antennas. (R. Hills, private communication). Fig. 9 illustrates the variation in effective antenna area over the frequency range.

3.3. Phase decorrelation

Phase errors can be incorporated into the sensitivity estimations via an efficiency η_p :

$$\eta_p = e^{-\phi(\nu)^2/2} \quad (5)$$

where $\phi(\nu)$ is the error on the phase (in radians) at the required frequency. The sensitivity limit for a given observation is then increased by a factor of $1/\eta_p$. For example, a phase error (after calibration) of 30° would correspond the an increase in the noise limit reached in a given integration time by a factor of 1.15. Phase errors will arise from residual atmospheric phase errors after calibration. Additionally, errors on the local oscillator phase could also contribute.

Details of the atmospheric phase stability at the Chajnantor ALMA site was examined in detail during the design of ALMA, and is documented in a variety of ALMA memos. See in particular the ALMA memos 365 and 471.

The phase noise was measured prior to the construction of ALMA using a 11.2 GHz site-test interferometer with a 300 m baseline looking at a geostationary satellite beacon at an airmass of $A = 1.7$ (Radford et al, 2003). This primary measurement we denote ϕ_{11} . To estimate the actual phase noise at other frequencies and on other

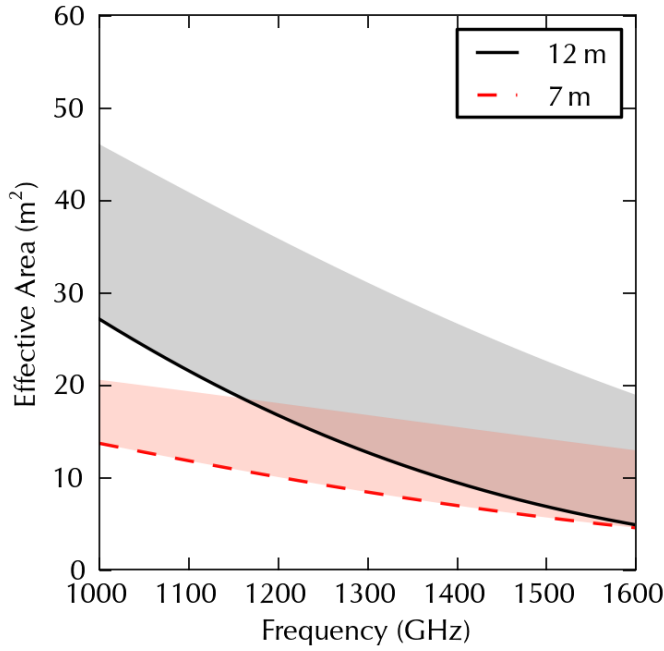


Figure 9: The effective area of the antennas for 12m (black) and 7m (red) antennas over the 1-1.6 THz region. The physical area of the dishes is 113.1 m^2 (12m) and 38.5 m^2 (7m). This assumes a smoothness of $25 \mu\text{m}$ (12m) and $20 \mu\text{m}$ (7m). The shaded area indicates the optimistically possible range if the antennas are found to have significantly exceeded their specification (up to $18 \mu\text{m}$ for the 12 m and up to $13 \mu\text{m}$ for the 7 m).

Table 3: Percentiles of the measured phase noise at 11.2 GHz on 300 m baselines, taken from ALMA Memo 471. An estimated conversion to THz wavelengths is included, assuming a scaling of $s = 0.6$ for the baseline conversion.

	measured ϕ_{rms} (300 m) 11.2 GHz	estimated					
		ϕ_{rms} (300 m)			ϕ_{rms} (32 m)		
		1022	1350	1501	1022	1350	1501
75%	5.3°	484°	639°	710°	127°	167°	185°
50%	2.5°	228°	301°	335°	60°	79°	87°
25%	1.2°	110°	145°	161°	29°	38°	42°
10%	0.7°	64°	84°	94°	17°	22°	25°

baselines, the equation from ALMA memo 471 is used, which assumes a simple Kolmogorov scaling of the atmospheric structure function, and no dispersion:

$$\phi_{\text{rms}}(A, \nu, b) = \phi_{11} \left(\frac{A}{1.7} \right)^{0.5} \left(\frac{\nu}{11.2 \text{ GHz}} \right) \left(\frac{b}{0.3 \text{ km}} \right)^s \quad (6)$$

where ϕ_{rms} is the root-mean-square phase noise, A is the airmass, ν is the frequency and b is the baseline length. As in Memo 471, we use $s = 0.6$ for estimating the variation with baseline length.

Converted to zenith observations, the measured percentiles for the phase noise from the atmosphere are given in Table 3, taken from ALMA Memo 471. In addition, an estimated conversion to the phase noise expected at THz frequencies is shown, for 300 m and 32 m baselines (following Eq. 6).

So using the 50 percentile measured phase noise of 2.5° towards zenith, this would correspond to a phase error of 60° at 1022 GHz (assuming $s = 0.6$ for a baseline of

32 m (ACA)), before any calibration is applied. The 10 percentile value of 0.7° would give a phase error of only 17° .

Phase calibration plans (such as fast-switching of observations or WVR calibration) should reduce these numbers, but the accuracy of the calibration will be an important limiting factor for THz observing with ALMA, particularly if attempts are made to use longer baseline configurations. The dispersive phase errors near the large number of absorption lines present in the THz windows are also a concern – see ALMA Memo 404 on the potential effects of dispersive phase and fast switching observations.

4. Sensitivity

The point source flux sensitivity (in Jansky) for ALMA can be estimated using:

$$\sigma_S = \frac{2kT_{\text{sys}}}{\eta_q \eta_c A_{\text{eff}} \sqrt{N(N-1) n_p \delta \nu t_{\text{int}}}} \quad (7)$$

and using the standard ALMA values from the ALMA technical handbook where appropriate. $\eta_q = 0.96$ is the quantisation efficiency, $\eta_c = 0.88$ is the correlator efficiency. The standard ALMA continuum mode has $\delta \nu$ of 7.5 GHz, and can have $n_p = 2$ ($n_p = 1$ is used for extremely high spectral resolution observations, not being considered here). The system temperature has been modelled previously for a range of weather conditions and receiver temperatures, and the effective antenna area (A_{eff}) is calculated above. These values can be used to estimate a point source sensitivity for a given number of antennas and a given integration time.

The point source surface brightness sensitivity (in K) can also be calculated from the point source flux sensitivity:

$$\sigma_T = \sigma_S \frac{c^2}{2k\nu^2 \Omega'} \quad (8)$$

where σ_T is the point source surface brightness sensitivity in K, σ_S is the point source flux sensitivity in Jy, ν is the frequency and Ω is the beam solid angle.

The beam solid angle is calculated from the half-power beam width θ of the array (in radians) via

$$\Omega = \frac{\pi \theta^2}{4 \ln 2}. \quad (9)$$

A number of sensitivity tables are presented which make different assumptions about the number of antennas N equipped with Band 11 receivers. The full ALMA antenna count is 50 12-m antennas in the main array, and 4 12-m plus 12 7-m antennas in the ACA. We include tables for $N = 6, 18, 54$ 12-m antennas, and $N = 6, 12$ 7-m antennas. This is not meant to imply that any of these values of N is preferred or realistic, but simply to give indicative figures for various potential configurations. It is perhaps likely that a Band 11 system would be prototyped on a small number of antennas first, and for this example we have chosen $N = 6$ inline with the Band 5 development: any fewer than this is likely to make imaging rather difficult. At the other extreme, it might be possible to equip all 54 antennas with Band 11 systems, although cross correlation of the ACA and main array antennas is not a routine mode of operation. Nonetheless, the three choices $N = 6, 18, 54$ neatly represent the range of performances possible with a Band 11 system.

4.1. Angular Resolution

The resolution of the array at a given frequency can be roughly estimated from the maximum baseline b of the array configuration as λ/b . For a range of maximum baselines, Table. 4 gives the associated angular resolution.

Table 4: The estimated resolution of the array over these THz frequencies for a range of maximum baselines. Note that the 32 m baselines are for the 7-m ACA only. The resolutions are given in arcseconds.

Max Baseline (m)	Resolution (arcseconds)			
	Frequencies (GHz)			
	1000	1200	1400	1600
32	1.93	1.61	1.38	1.21
150	0.41	0.34	0.29	0.26
500	0.12	0.10	0.09	0.08
1000	0.06	0.05	0.04	0.04
5000	0.01	0.01	0.01	0.01

4.2. Flux Sensitivity Estimates: 1000 K

For a constant (across the band) receiver noise of 1000 K, a zenith angle of 15 degrees, the point-source flux sensitivity of a variety of antenna configurations has been estimated for 1 s, 1 min and 1 hr observations, for PWV values of 200, 300 and 500 μm .

6x7 m antennas

ν GHz	PWV μm	σ_s (Jy)		
		1 s	1 min	1 hr
1022	200	1.5	0.20	0.025
1022	300	2.6	0.33	0.043
1022	500	7.1	0.92	0.12
1350	200	2.6	0.34	0.044
1350	300	4.5	0.58	0.075
1350	500	13	1.7	0.22
1501	200	3.6	0.47	0.060
1501	300	6.2	0.79	0.10
1501	500	17	2.2	0.29

12x7 m antennas

ν GHz	PWV μm	σ_S (Jy)		
		1 s	1 min	1 hr
1022	200	0.72	0.093	0.012
1022	300	1.2	0.16	0.020
1022	500	3.4	0.44	0.057
1350	200	1.2	0.16	0.021
1350	300	2.2	0.28	0.036
1350	500	6.2	0.80	0.10
1501	200	1.7	0.22	0.029
1501	300	2.9	0.38	0.049
1501	500	8.3	1.1	0.14

6x12 m antennas

ν GHz	PWV μm	σ_S (Jy)		
		1 s	1 min	1 hr
1022	200	0.78	0.10	0.013
1022	300	1.3	0.17	0.022
1022	500	3.7	0.47	0.061
1350	200	1.8	0.24	0.031
1350	300	3.2	0.41	0.053
1350	500	9.1	1.2	0.15
1501	200	3.0	0.39	0.050
1501	300	5.1	0.66	0.085
1501	500	14	1.9	0.24

18x12 m antennas

ν GHz	PWV μm	σ_S (Jy)		
		1 s	1 min	1 hr
1022	200	0.24	0.032	0.0041
1022	300	0.41	0.053	0.0069
1022	500	1.2	0.15	0.019
1350	200	0.57	0.074	0.0096
1350	300	0.99	0.13	0.016
1350	500	2.9	0.37	0.048
1501	200	0.94	0.12	0.016
1501	300	1.6	0.21	0.027
1501	500	4.5	0.58	0.075

54x12 m antennas

ν GHz	PWV μm	σ_s (Jy)		
		1 s	1 min	1 hr
1022	200	0.080	0.010	0.0013
1022	300	0.13	0.017	0.0022
1022	500	0.38	0.049	0.0063
1350	200	0.19	0.024	0.0031
1350	300	0.32	0.042	0.0054
1350	500	0.94	0.12	0.016
1501	200	0.31	0.040	0.0051
1501	300	0.52	0.068	0.0087
1501	500	1.5	0.19	0.025

4.3. Surface Brightness Temperature estimates

As for the flux sensitivity estimates above, for a constant receiver noise temperature of 1000 K and a source angle of 15 degrees, the surface brightness sensitivity (in Kelvin) has been predicted for a variety of different antenna number and configurations. The calculations have been made for 1 hr observations in 0.5 and 20 km/s channel widths, using PWV values of 200, 300 and 500 μm , and looking at 32 m baselines (7 m antennas) and 150, 500, 1000 and 5000 m baselines (12 m antennas). It was assumed that the antenna smoothness was equal to the specification value.

6x7 m antennas at 32 m maximum baseline

ν GHz	PWV μm	σ_K (K) 0.5km/s			σ_K (K) 20km/s		
		1 s	1 min	1 hr	1 s	1 min	1 hr
1022	200	33	4.2	0.55	5.2	0.67	0.087
1022	300	56	7.2	0.93	8.8	1.1	0.15
1022	500	150	20	2.6	25	3.2	0.41
1350	200	49	6.4	0.82	7.8	1.0	0.13
1350	300	85	11	1.4	13	1.7	0.22
1350	500	250	32	4.1	39	5.0	0.65
1501	200	65	8.4	1.1	10	1.3	0.17
1501	300	110	14	1.8	17	2.2	0.29
1501	500	310	40	5.2	49	6.3	0.82

12x7 m antennas at 32 m maximum baseline

ν GHz	PWV μm	σ_K (K) 0.5km/s			σ_K (K) 20km/s		
		1 s	1 min	1 hr	1 s	1 min	1 hr
1022	200	16	2.0	0.26	2.5	0.32	0.041
1022	300	27	3.4	0.44	4.2	0.54	0.070
1022	500	74	9.5	1.2	12	1.5	0.19
1350	200	24	3.0	0.39	3.7	0.48	0.062
1350	300	41	5.2	0.68	6.4	0.83	0.11
1350	500	120	15	2.0	19	2.4	0.31
1501	200	31	4.0	0.52	4.9	0.63	0.082
1501	300	53	6.8	0.88	8.3	1.1	0.14
1501	500	150	19	2.5	23	3.0	0.39

6x12 m antennas,3600.0 s integration time

ν GHz	PWV μm	σ_K (K) 0.5 km/s			σ_K (K) 20 km/s		
		150 m	500 m	1000 m	150 m	500 m	1000 m
1022	200	5.6	62	250	0.88	9.8	39
1022	300	9.4	100	420	1.5	17	66
1022	500	26	290	1200	4.1	46	180
1350	200	12	140	550	2.0	22	87
1350	300	21	240	940	3.4	37	150
1350	500	60	670	2700	9.5	110	420
1501	200	20	220	870	3.1	34	140
1501	300	33	370	1500	5.2	58	230
1501	500	93	1000	4100	15	160	660

18x12 m antennas,3600.0 s integration time

ν GHz	PWV μm	σ_K (K) 0.5 km/s			σ_K (K) 20 km/s		
		150 m	500 m	1000 m	150 m	500 m	1000 m
1022	200	1.7	19	78	0.28	3.1	12
1022	300	2.9	33	130	0.47	5.2	21
1022	500	8.2	91	360	1.3	14	57
1350	200	3.9	43	170	0.62	6.8	27
1350	300	6.6	74	300	1.0	12	47
1350	500	19	210	840	3.0	33	130
1501	200	6.1	68	270	0.97	11	43
1501	300	10	120	460	1.6	18	73
1501	500	29	320	1300	4.6	51	210

54x12 m antennas,3600.0 s integration time

ν GHz	PWV μm	σ_K (K) 0.5 km/s			σ_K (K) 20 km/s		
		150 m	500 m	1000 m	150 m	500 m	1000 m
1022	200	0.57	6.3	25	0.090	1.0	4.0
1022	300	0.96	11	43	0.15	1.7	6.8
1022	500	2.7	30	120	0.42	4.7	19
1350	200	1.3	14	57	0.20	2.2	8.9
1350	300	2.2	24	97	0.34	3.8	15
1350	500	6.2	69	270	0.98	11	43
1501	200	2.0	22	89	0.32	3.5	14
1501	300	3.4	38	150	0.54	6.0	24
1501	500	9.5	110	420	1.5	17	67

4.4. 500 K Receiver temperature Flux Sensitivity

As a comparison, the same sensitivity calculations as before were also done assuming a receiver temperature of 500 K.

6x7 m antennas

ν GHz	PWV μm	σ_s (Jy)		
		1 s	1 min	1 hr
1022	200	0.86	0.11	0.014
1022	300	1.5	0.19	0.025
1022	500	4.2	0.54	0.070
1350	200	1.5	0.19	0.024
1350	300	2.6	0.33	0.043
1350	500	7.6	0.98	0.13

12x7 m antennas					18x12 m antennas				
ν	PWV	σ_s (Jy)			ν	PWV	σ_s (Jy)		
GHz	μm	1 s	1 min	1 hr	GHz	μm	1 s	1 min	1 hr
1022	200	0.41	0.053	0.0068	1022	200	0.14	0.018	0.0023
1022	300	0.70	0.091	0.012	1022	300	0.24	0.031	0.0040
1022	500	2.0	0.26	0.033	1022	500	0.67	0.087	0.011
1350	200	0.70	0.090	0.012	1350	200	0.32	0.042	0.0054
1350	300	1.2	0.16	0.020	1350	300	0.56	0.073	0.0094
1350	500	3.6	0.47	0.060	1350	500	1.7	0.21	0.028
1501	200	0.97	0.12	0.016	1501	200	0.53	0.068	0.0088
1501	300	1.7	0.22	0.028	1501	300	0.91	0.12	0.015
1501	500	4.8	0.62	0.080	1501	500	2.6	0.34	0.043

6x12 m antennas					54x12 m antennas				
ν	PWV	σ_s (Jy)			ν	PWV	σ_s (Jy)		
GHz	μm	1 s	1 min	1 hr	GHz	μm	1 s	1 min	1 hr
1022	200	0.44	0.057	0.0073	1022	200	0.045	0.0058	0.00075
1022	300	0.76	0.098	0.013	1022	300	0.078	0.010	0.0013
1022	500	2.1	0.28	0.036	1022	500	0.22	0.028	0.0037
1350	200	1.0	0.13	0.017	1350	200	0.11	0.014	0.0018
1350	300	1.8	0.23	0.030	1350	300	0.18	0.024	0.0031
1350	500	5.3	0.68	0.088	1350	500	0.54	0.070	0.0090
1501	200	1.7	0.22	0.028	1501	200	0.17	0.022	0.0029
1501	300	2.9	0.37	0.048	1501	300	0.30	0.038	0.0050
1501	500	8.3	1.1	0.14	1501	500	0.85	0.11	0.014

4.5. 500 K Receiver temperature Surface Brightness

And similarly the surface brightness sensitivity was also estimated for 500 K.

6x7 m antennas at 32 m maximum baseline

ν	PWV	σ_K (K) 0.5km/s			σ_K (K) 20km/s		
		1 s	1 min	1 hr	1 s	1 min	1 hr
1022	200	19	2.4	0.31	2.9	0.38	0.049
1022	300	32	4.1	0.53	5.1	0.65	0.084
1022	500	91	12	1.5	14	1.8	0.24
1350	200	28	3.6	0.46	4.4	0.57	0.073
1350	300	49	6.3	0.81	7.7	0.99	0.13
1350	500	140	18	2.4	23	2.9	0.38
1501	200	36	4.7	0.60	5.7	0.74	0.096
1501	300	63	8.1	1.0	9.9	1.3	0.17
1501	500	180	23	3.0	28	3.7	0.47

12x7 m antennas at 32 m maximum baseline

ν GHz	PWV μm	$\sigma_K(\text{K})$ 0.5km/s			$\sigma_K(\text{K})$ 20km/s		
		1 s	1 min	1 hr	1 s	1 min	1 hr
1022	200	8.9	1.1	0.15	1.4	0.18	0.023
1022	300	15	2.0	0.25	2.4	0.31	0.040
1022	500	43	5.6	0.72	6.8	0.88	0.11
1350	200	13	1.7	0.22	2.1	0.27	0.035
1350	300	23	3.0	0.39	3.7	0.47	0.061
1350	500	68	8.8	1.1	11	1.4	0.18
1501	200	17	2.2	0.29	2.7	0.35	0.046
1501	300	30	3.9	0.50	4.7	0.61	0.079
1501	500	86	11	1.4	14	1.7	0.23

6x12 m antennas,3600.0 s integration time

ν GHz	PWV μm	σ_K (K) 0.5 km/s			σ_K (K) 20 km/s		
		150 m	500 m	1000 m	150 m	500 m	1000 m
1022	200	3.1	35	140	0.50	5.5	22
1022	300	5.4	60	240	0.85	9.5	38
1022	500	15	170	680	2.4	27	110
1350	200	7.0	77	310	1.1	12	49
1350	300	12	130	540	1.9	21	85
1350	500	35	390	1600	5.5	62	250
1501	200	11	120	490	1.7	19	77
1501	300	19	210	840	3.0	33	130
1501	500	54	600	2400	8.5	95	380

18x12 m antennas,3600.0 s integration time

ν GHz	PWV μm	σ_K (K) 0.5 km/s			σ_K (K) 20 km/s		
		150 m	500 m	1000 m	150 m	500 m	1000 m
1022	200	0.98	11	44	0.16	1.7	6.9
1022	300	1.7	19	75	0.27	3.0	12
1022	500	4.8	53	210	0.76	8.4	34
1350	200	2.2	24	97	0.34	3.8	15
1350	300	3.8	42	170	0.60	6.7	27
1350	500	11	120	490	1.7	19	77
1501	200	3.4	38	150	0.54	6.0	24
1501	300	5.9	66	260	0.93	10	42
1501	500	17	190	750	2.7	30	120

54x12 m antennas, 3600.0 s integration time

ν GHz	PWV μm	σ_K (K) 0.5 km/s			σ_K (K) 20 km/s		
		150 m	500 m	1000 m	150 m	500 m	1000 m
1022	200	0.32	3.6	14	0.051	0.56	2.3
1022	300	0.55	6.1	25	0.087	0.97	3.9
1022	500	1.6	17	69	0.25	2.7	11
1350	200	0.71	7.9	32	0.11	1.3	5.0
1350	300	1.2	14	55	0.20	2.2	8.7
1350	500	3.6	40	160	0.57	6.3	25
1501	200	1.1	12	50	0.18	2.0	7.9
1501	300	1.9	21	86	0.31	3.4	14
1501	500	5.5	61	250	0.87	9.7	39

4.6. Receiver Temperature

The above sensitivities were all calculated for a constant receiver temperature. The variation of sensitivity with receiver temperature is shown in Fig. 10, for the case of 18 12-m antennas on 150 m baselines at 1350 GHz, for a 1 hour integration time. Flux sensitivity was calculated over 7.5 GHz, and brightness sensitivity over a 0.5 km/s channel.

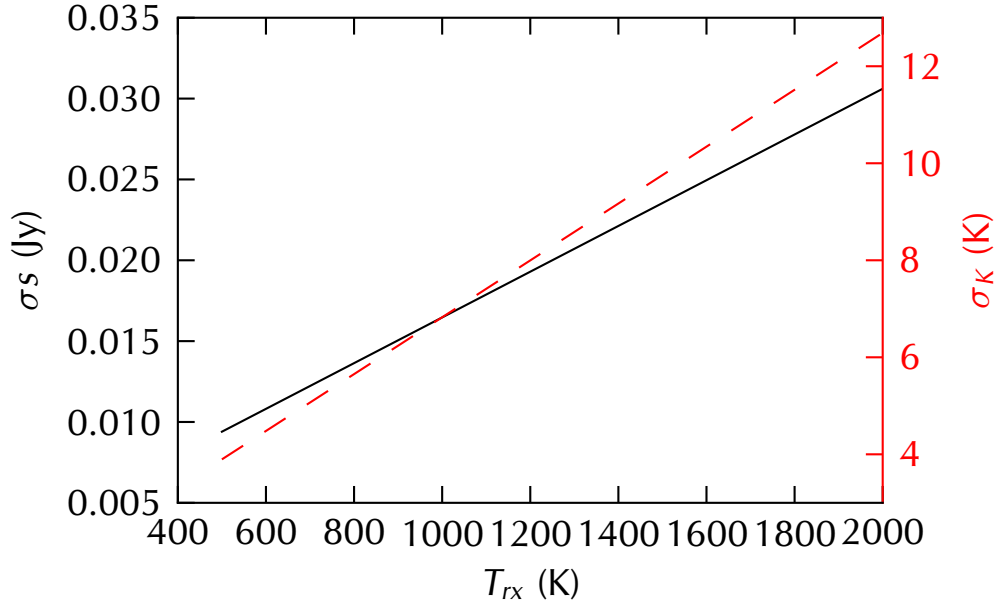


Figure 10: Variation of point source flux sensitivity (σ_s) and surface brightness sensitivity (σ_K) for varying receiver temperatures, at 1350 GHz with 1 hour integration on 18 12 m antennas with a maximum baseline of 150 m. σ_s calculated for 7.5 GHz continuum, and σ_K for a 0.5 km/s channel.

5. Phase Calibration

Traditional millimeter wave interferometric phase calibration involves switching to observations of a phase calibrator source at regular intervals. The phase calibrator is ideally an extremely bright and constant point source with an assumed phase of 0. Therefore the measured phase on the calibrator is subtracted from the observed

phase on the target. To calibrate away the atmospheric effects, the calibrator needs to be observed at a timescale equivalent to that of the atmospheric fluctuations.

The current and proposed ALMA phase calibration methods include:

- Traditional interferometric phase calibration: regular (slow) observing of a phase calibrator (traditionally a quasar). This only calibrates out atmospheric fluctuations at the time scale of the switching or longer, so is not useful for rapid phase errors due primarily to small scale water inhomogeneities in the atmosphere.
- WVR observing: all 12m antennas take 183 GHz WVR observations during all observations, at a 1 s sampling rate. This allows calculation of the variation in water emission from the atmosphere during an observation. Its main limitations are that it doesn't measure dry fluctuations, and dispersion needs careful correction. Observations for 7m antennas have to be estimated from the 12m observations as they don't have WVR units.
- Fast-switching phase correction scheme. This is essentially the same as the standard and currently implemented phase calibration, except it switches very regularly to the calibrator (on the scales of tens of seconds). This method requires a bright calibrator that is very close in the sky to the science target. This is the best possible scheme in terms of efficiency and accuracy if the system can switch fast enough and the calibrator is very nearby.
- Fast switching plus WVR calibration: this scheme holds the most promise for accurate phase calibration, and is being commissioned at ALMA: it requires improvements to the software to enable fast switching of the antennas.
- Phase frequency transfer: in this scheme, when ALMA switches to a calibrator, it also retunes to band 3 (3mm), and measures the phase on a quasar at this low frequency. The phase is then scaled to high frequency and applied to the source. This requires excellent electrical stability of the system and has great potential, although I have yet to see many results. Its key advantage is the large number of 3mm-bright quasars in the sky.

Given the poor atmospheric transparency at these frequencies, some form of fast switching observations seems essential for THz observing with ALMA. However, finding bright, THz calibration sources will be extremely difficult, particularly as the high angular resolution of ALMA at these frequencies will resolve many traditional sub/mm calibrators. Quasars do not tend to be bright at these frequencies: ALMA memo 520 (Holdaway & Owen, 2005) produced estimated source counts of less than 1 per steradian for 1 Jy flat-spectrum quasars at 900 GHz. For fast switching this problem is compounded, as the calibrators must be reasonably close to the source in order to allow for the very frequent slewing between the sources.

Phase transfer of calibrator sources is planned to be implemented on the telescope, and this would massively open up the range of feasible calibrators. Assuming it can be combined with fast switching, this should allow calibration of the atmospheric phase, and massively improve the amplitude loss through phase decoherence discussed in section 4.3

5.1. Calibrator source sensitivity

Using the standard source sensitivity equation described earlier, and assuming $300 \mu\text{m}$ PWV, a receiver temperature of 1000 K, and an integration of 1s and all other values as previously, a single baseline on two 12 m antennas at specification ($N = 2$) will have a sensitivity in the 1 THz window of 5.1 Jy. In 10 s this would rise to 1.6 Jy. These numbers make it clear that observing at THz frequencies with fast switching will require

the telescope to have implemented transfer of phase from low frequencies.

5.2. Alternate sources

Asteroids and the Galilean moons have been used as submm/mm flux calibrators, although not traditionally as phase calibrators. However, although their size is not ideal, given the difficulty of calibration at these wavelengths they should be considered as possibilities, and are fairly bright at THz wavelengths.

The Galilean moons, Io, Callisto, Ganymede and Europa have angular sizes of ≈ 1.3 - 0.7 arcseconds. The CASA `set_solar_system_fd` task calculates their flux densities at 1 THz as between 20 and 70 Jy. Specifically these were Io:30-65 Jy at 0.8-1.2'', Callisto: 60-140 Jy at 1-1.6''; Ganymede: 65-150 Jy at 1.1-1.7''; Europa: 20-45 at 0.75-1''. The brightness temperature models used for this calculation are described in Butler 2012 (ALMA Memo 594). Note that this warns that the brightness temperatures of Io and Europa are extremely poorly constrained.

Asteroids have also been used as calibration targets in the IR (see e.g. T Muller's contribution to the Herschel calibration workshop), and as interferometric flux calibrators. The CASA task to calculate their flux density assumes a constant brightness temperature, so cannot be considered the most reliable method. The size and flux density also naturally vary with time. However, this method calculates densities of 10-60 Jy (Ceres, 0.4-0.8''), 3-35 Jy (Pallas, 0.2-0.6''), 4-30 Jy (Vesta, 0.2-0.65'') and 0.5-45 Jy (Juno, 0.08-0.25''). These may be a little high, based on the Herschel SPIRE measurements of Ceres and Pallas, but nonetheless are worth pursuing as potential calibrators at Band 11.

5.3. Dispersion

Atmospheric dispersion in the ALMA observing bands is significant, has implications for phase correction if it is done by phase transfer or using water-vapour based corrections. However this is a tractable problem that has been studied extensively in ALMA Memos 590 and 404: it simply requires the dispersion to be calculated using the atmospheric model, and both the `am` and `ATM` packages can do this accurately. These *ab initio* calculations will then need checking using real commissioning observations with Band 11. Before then, we should be able to learn a lot from the Band 10 system where the same issue arises. This will no doubt inform the approach for band 11 calibration and observing strategy — the extrapolation from Band 10 to Band 11 is rather modest in this context.

5.4. Amplitude Calibration

We have not been able to quantify in this work the effect of *amplitude* errors caused by atmospheric absorption fluctuations, but we note here that these are an important source of error that will need further investigation. It should be possible to make some progress on this by taking the existing 183-GHz measurements from ALMA at high time resolution and, using the atmospheric radiative transfer code, make predictions of the size of these amplitude errors. These can then be included in the full imaging simulations performed later in this report. A second piece of information will come from the Band 10 commissioning observations on ALMA which should permit a more direct estimate of the size of these errors at a frequency comparable to Band 11.

5.5. Phase Calibration Summary

Based on the current state of knowledge, fast switching and phase transfer will be required for accurate, high-fidelity calibration at these frequencies. In addition, effort will be required to correct for the dispersive and dry atmospheric effects. There has not as yet been a large amount of work on WVR calibration in extremely good weather, so it is not clear how much it will improve matters when there is so little water in the atmosphere. However, in the time while band 11 is being considered and planned, further work will have been carried out on Band 10 observing. This experience will be very valuable in guiding the observation and calibration strategy for Band 11 observations. This is rather an unknown. The possibility of using Asteroids or Galileans moons as calibrators should also be evaluated and tested at band 10 and 11 frequencies.

6. Imaging Simulations

It is important to assess the imaging performance of a Band 11 system on ALMA. To this end, we have made alterations to the code of the CASA `simobserve` task to permit simulations of THz imaging performed with ALMA. We simulate (a) a point source and (b) a complex image of a filamentary star forming region to help understand the imaging performance.

This simulation takes in a sky model of the object to be observed, allows the user to specify the sky brightness and opacity at zenith, the direction of the source, the number of pointings, the integration time, the size of the pixels in arcseconds (i.e. effectively the distance to the source), the time of the observation and the configuration of the telescope.

Initially, we make simulations assuming a receiver temperature of 1000 K, and add no phase degradation (i.e. assuming perfect phase correction). This can be seen in Fig. 11. All the simulations presented have 4 panels, clockwise from top left: 1) the sky image being observed, 2) the sky image convolved with the ALMA beam, 3) the residual noise and 4) the simulated image.

The noise was compared with the results of the simulations by simulating a region of blank sky for a 100s integration at transit (with a zenith angle of 0 degrees). The results were found to be very similar (our calculation gives an expected sensitivity of 0.0163 Jy, and averaging the results from 10 separately seeded blank sky 100s integration simulations gave a calculated standard deviation of 0.0157 Jy/beam in the central region of the simulated observation). This was despite slightly differing methods of calculation for e.g. the system temperature, and some small variations in the assumptions of the telescope efficiencies.

The sources were observed using the ACA (very compact, 7m ALMA antennas) array, and a compact configuration of 50 12m ALMA antennas. Three sources have been looked at: a point source, a source chosen to be representative of filamentary structure in a molecular cloud, and a protoplanetary disc model. These models were all simulated with an observing set up of 1021.5 GHz using 7.5 GHz bandwidth continuum mode.

The brightness of the sources presented in these simulations is set within the code and is not strongly physically motivated – it was chosen to allow the source to be detected in one run.

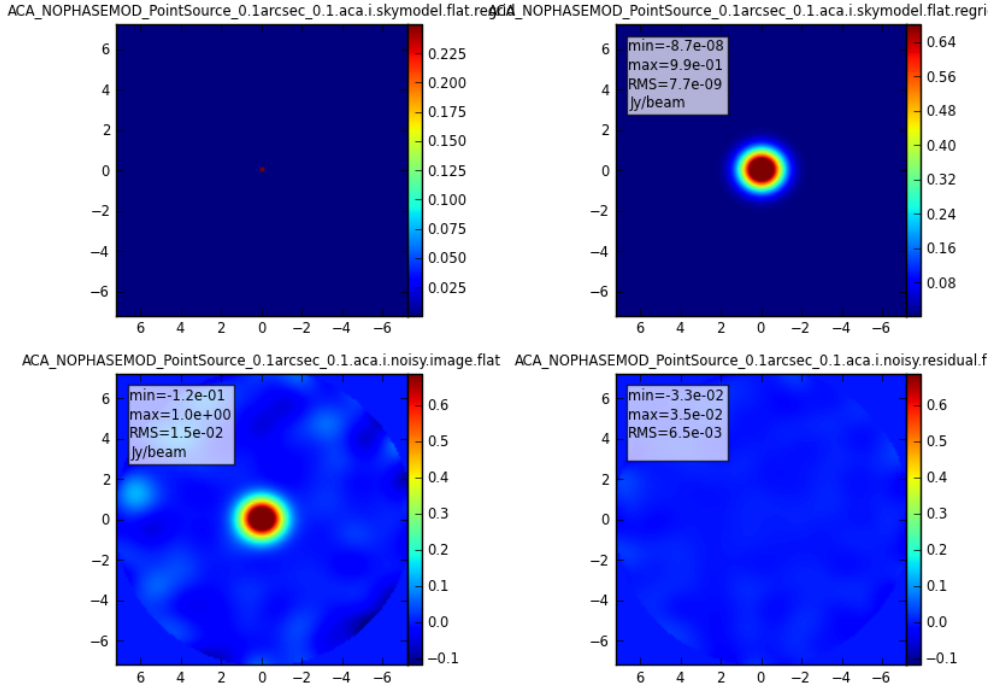


Figure 11: Point source observed with ACA: no additional phase errors. $\phi_{11} = 0^\circ$

6.1. Phase noise

To add phase noise, we first choose a value of ϕ_{11} (defined earlier) for the simulation: ϕ_{11} is the phase rms measured at 11 GHz, for which we have statistical information. We then use Eqn. 6 to scale this to the appropriate baseline, airmass and frequency. A standard simulation has been carried out using the atmospheric 10th phase error of $\phi_{11} = 0.7^\circ$. This is the performance expected in the top 10% of atmospheric stability *assuming no short-term phase correction is done*. This is of course somewhat pessimistic.

In addition, to illustrate imaging with phase some correction applied, we simulate in the same way but choose a lower value of ϕ_{11} , because we still expect the phase errors to grow with baseline, based on experience at lower frequencies. Typically we set $\phi_{11} = 0.1^\circ$ to illustrate the effect of imaging with some phase correction applied. This corresponds to a phase error of about 10° on 300-m baselines near to 1 THz.

6.2. Point Source

This source is a 1 Jy point source. It is observed for 7200 s in a single stare. It has been simulated with the ACA and a compact ALMA configuration with no additional phase errors ($\phi_{11} = 0.7^\circ$) errors at 300 m baseline on 11 GHz, and with 0.1° phase error at the same setup.

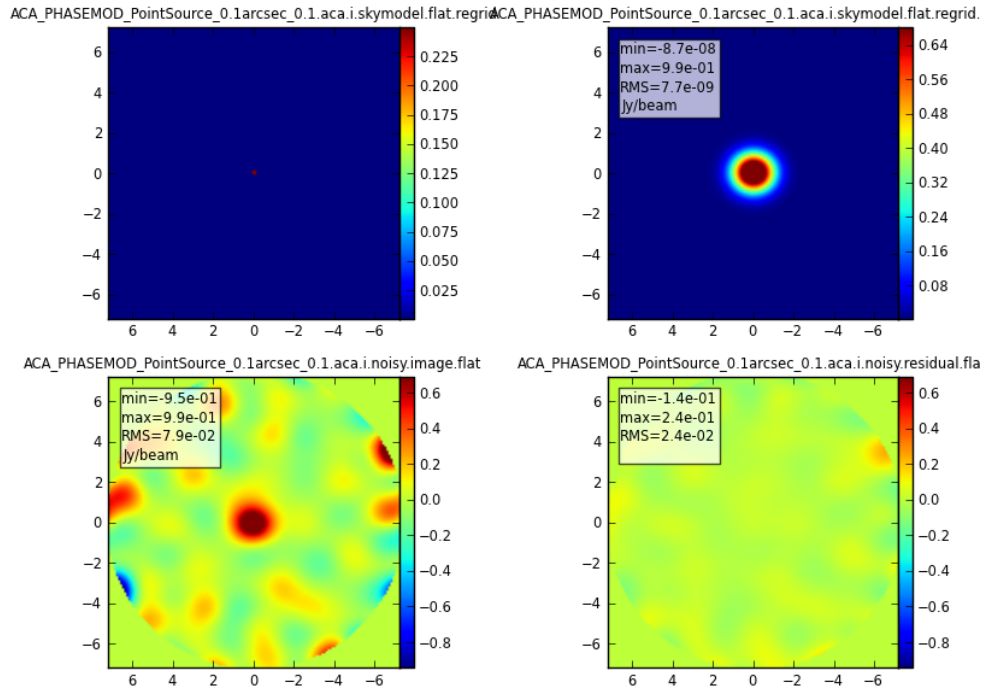


Figure 12: Point source observed with ACA: $\phi_{11}=0.1^\circ$

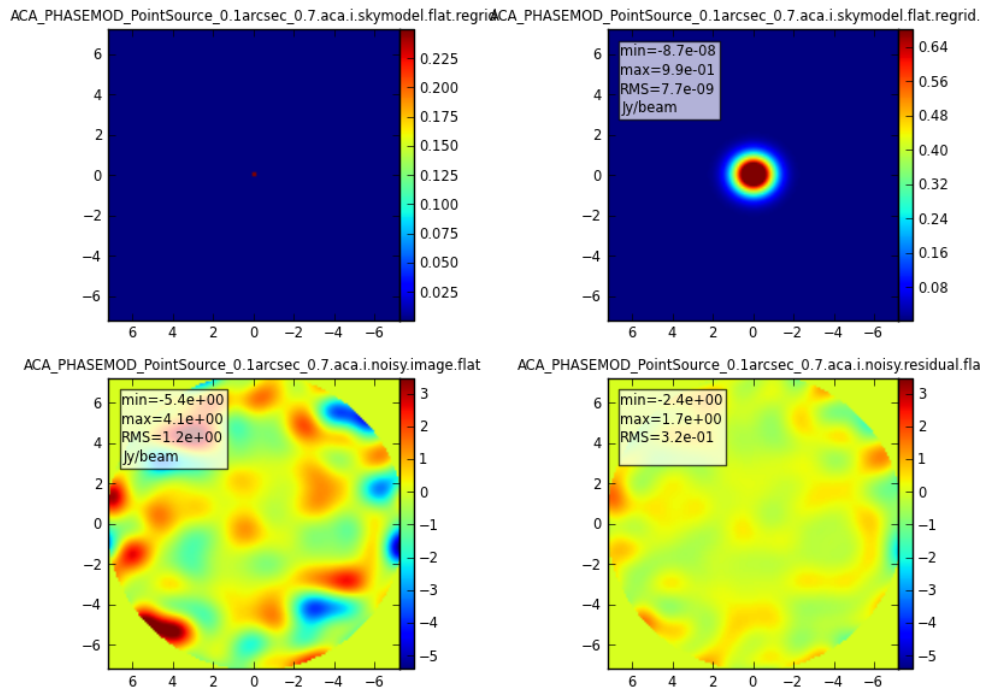


Figure 13: Point source observed with ACA: $\phi_{11}=0.7^\circ$

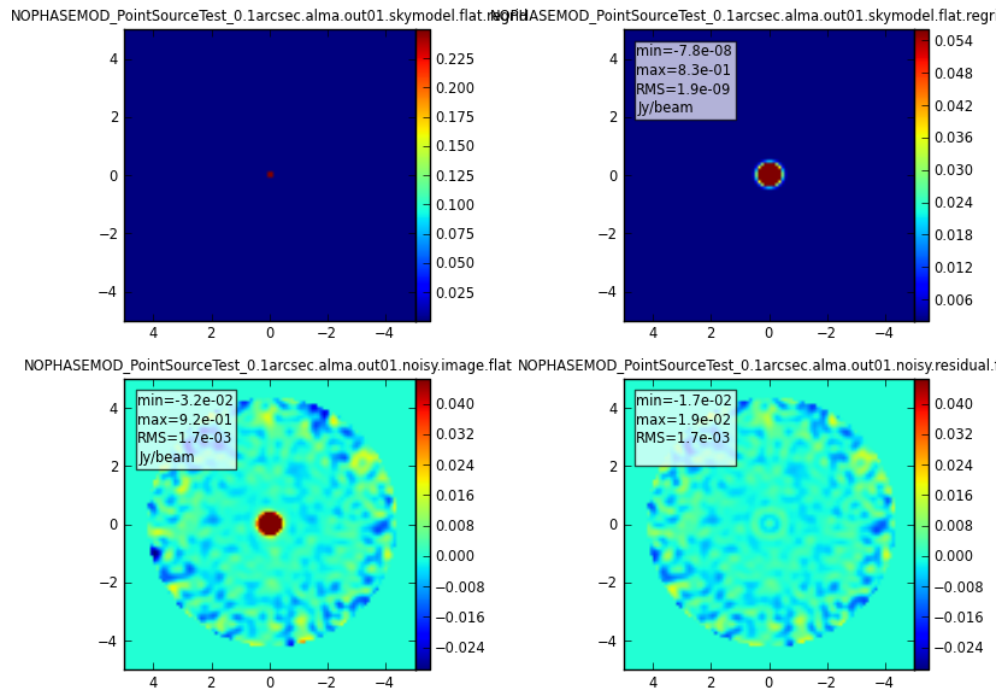


Figure 14: Point source observed with compact full ALMA: $\phi_{11}=0^\circ$

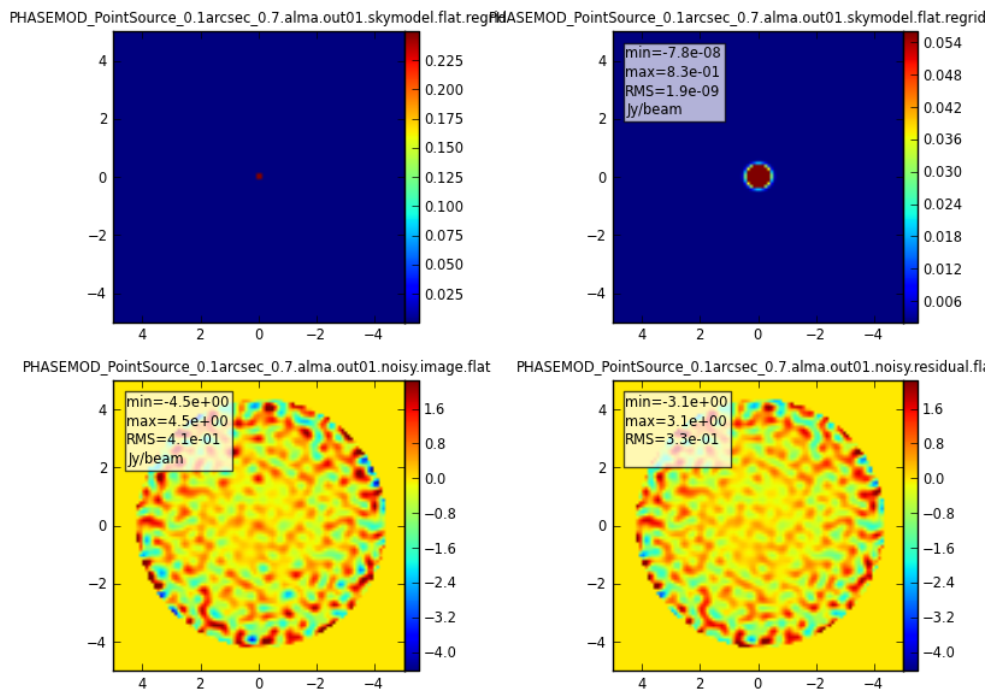


Figure 15: Point source observed with compact full ALMA: $\phi_{11}=0.7^\circ$

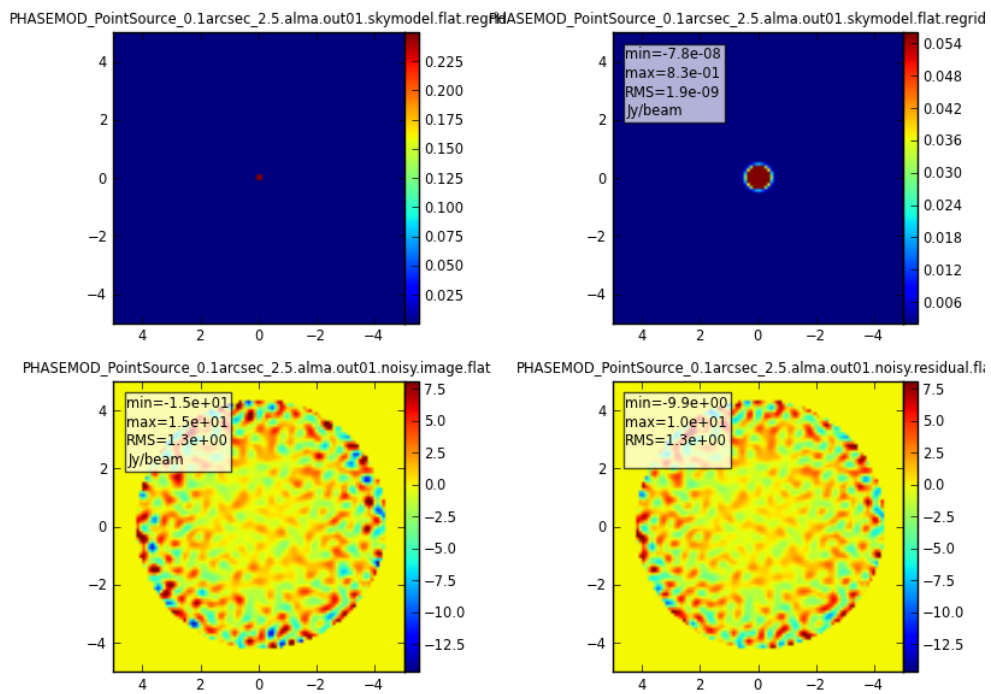


Figure 16: Point source observed with compact full ALMA: $\phi_{11} = 2.5^\circ$

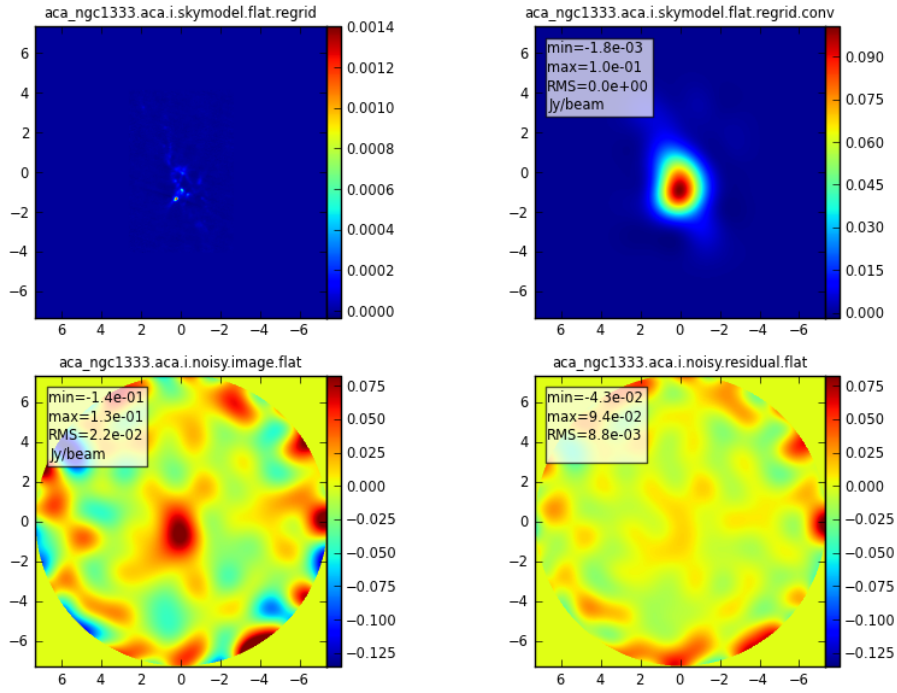


Figure 17: Filamentary source observed with ACA: $\phi_{11}=0^\circ$

6.3. A complex source: filamentary structure

A submm image of NGC1333 was used to test imaging of complex filamentary structure. This has been scaled to a peak flux of 0.0014Jy in a 0.03 arcsecond pixel. It is observed for 144000 s in 60s samples. It has been simulated with the ACA and a compact ALMA configuration with no additional phase errors, assuming the ten percentile value of 0.7° phase errors at 300 m baseline on 11 GHz, and with 0.1° phase error at the same setup.

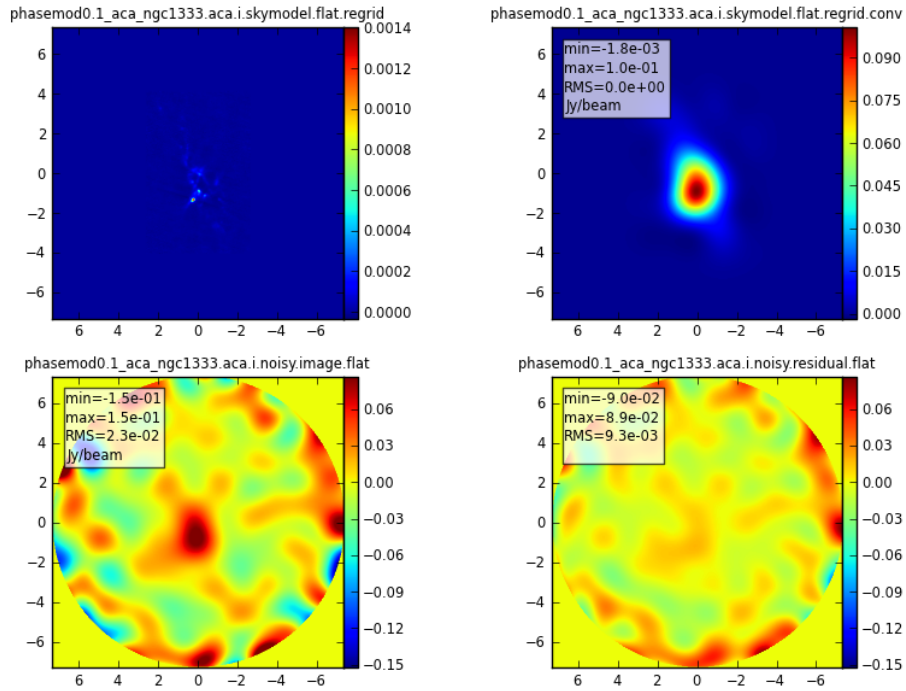


Figure 18: Filamentary source observed with ACA: $\phi_{11}=0.1^\circ$

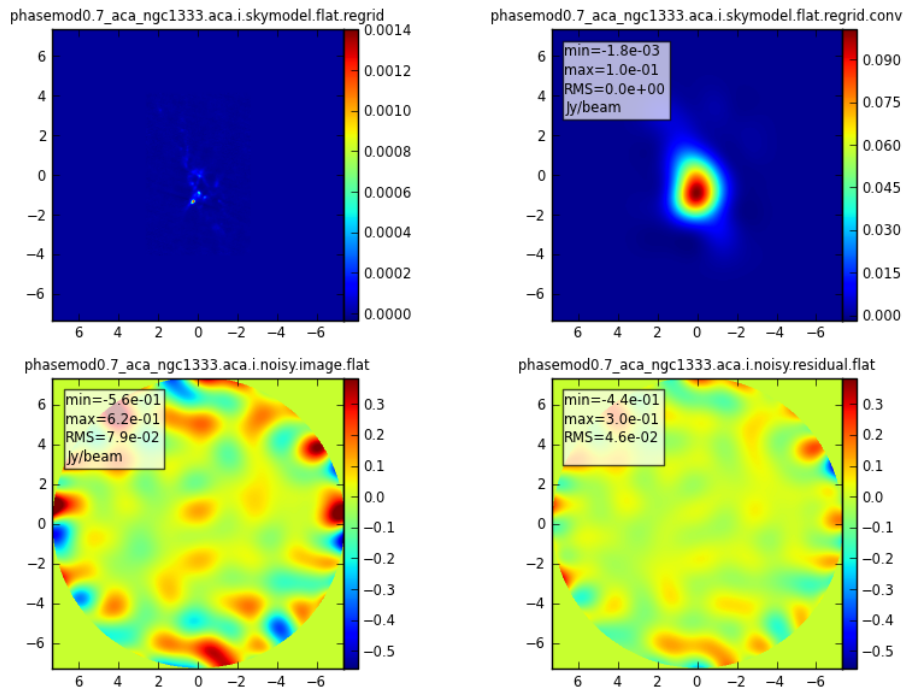


Figure 19: Filamentary source observed with ACA: $\phi_{11}=0.7^\circ$

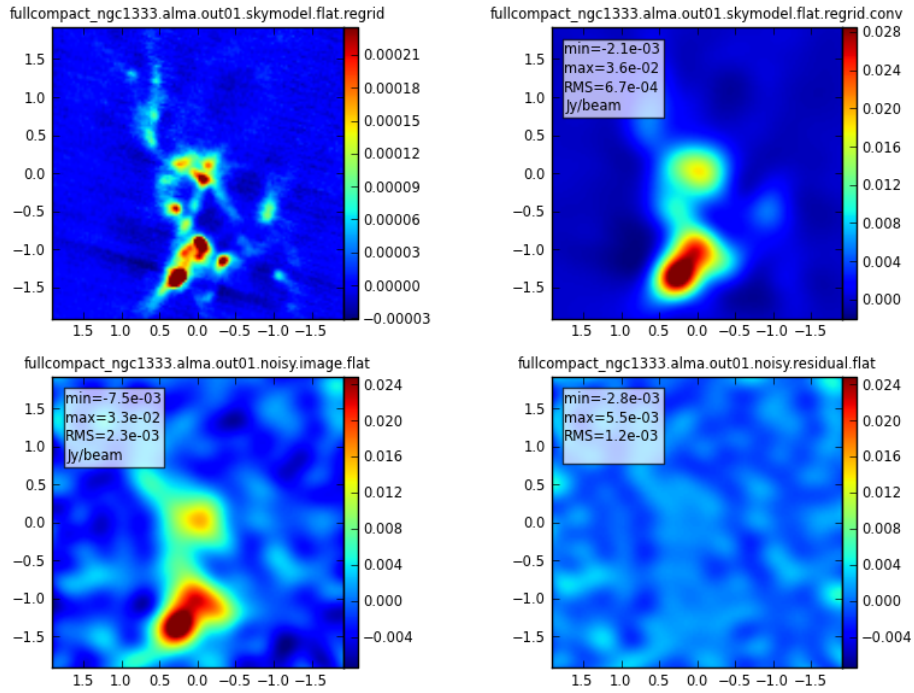


Figure 20: Filamentary source observed with compact full ALMA: $\phi_{11}=0^\circ$

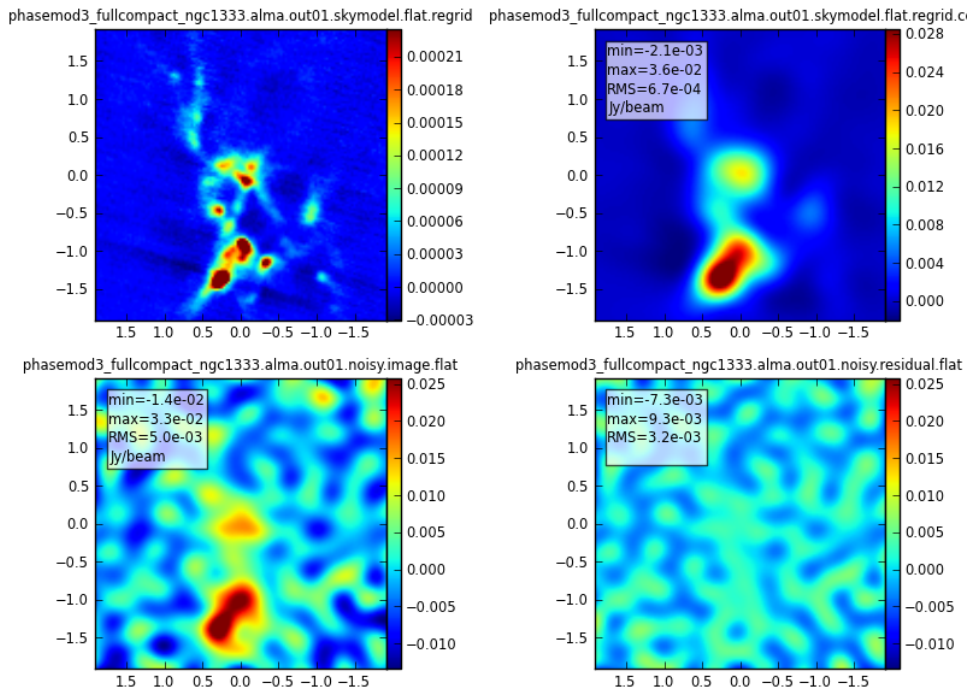


Figure 21: Filamentary source observed with compact full ALMA: $\phi_{11}=0.1^\circ$

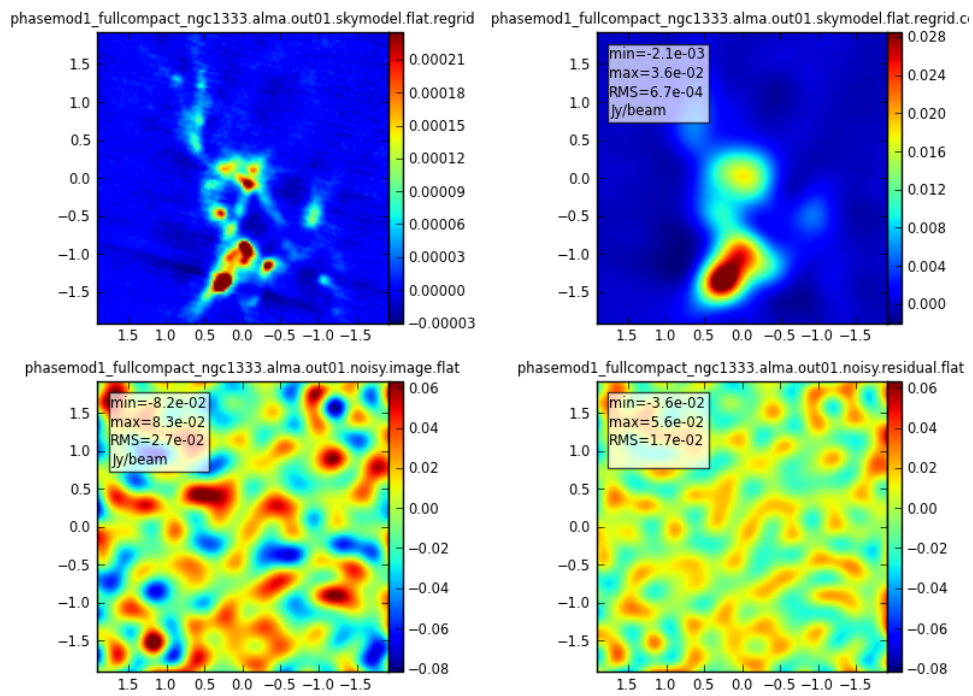


Figure 22: Filamentary source observed with compact full ALMA: $\phi_{11}=0.7^\circ$

7. Concluding Remarks

This report has presented some simple estimates of imaging performance and expected sensitivity of an ALMA Band 11 system. We stress that these are somewhat idealised and may not be achieved in practice — in particular, they make optimistic assumptions about the ability to accurately calibrate phase and amplitude at these very high frequencies, and that the primary beam can be predicted based on the known low-frequency holography measurements. Nonetheless they do show that Band 11 on ALMA has great possibilities if the calibration issues can be overcome. And not surprisingly they demonstrate that the crucial aspect for imaging will be the accuracy of the phase corrections: short baseline observations in the very best weather should present few difficulties, but beyond a few hundred meters in baseline length, we will need a very good fast switching plus WVR calibration scheme. Even then, we may be restricted to sources close to known bright THz calibrators, unless phase transfer from 3mm can be achieved with the ALMA system. Although further simulations could of course be pursued, it is perhaps wise at this stage to wait for quantitative data from the ALMA Band 10 system which will inform us rather well what to expect at frequencies above 1 THz.